(Received 15 June 2026, Accepted 19 July 2026, Scheduled 8 August 2026)

Disturbance Observer-Based Deadbeat Model Predictive Current Control for Permanent Magnet Synchronous Motor

Qing Lu, Linfeng Lv, Wan Chen*, and Tao Zhang

Faculty of Automation, Huai'an University, Huai'an, China

ABSTRACT: To address the issues of weak disturbance-rejection capability and poor parameter robustness in traditional model predictive control, a deadbeat model predictive current-control strategy with an improved disturbance observer is proposed. First, an active disturbance rejection controller is designed to replace the PI control, achieving both fast response and overshoot-free performance during speed tracking. Then, the influence of parameter disturbances on motor control performance in conventional model predictive control is analyzed, and a disturbance observer with adaptively adjustable gain is designed. The parameter mismatch disturbances can be compensated. Therefore, the current ripple can be significantly suppressed, and the robustness of the system parameters can be enhanced. Finally, the performance of the proposed method was demonstrated through simulations and experiments.

1. INTRODUCTION

Permanent magnet synchronous motor (PMSM) is a high-order, nonlinear, and strongly coupled system. With the development of permanent magnet materials, they have been widely used in fields such as vehicles, industrial servos, and aerospace due to their high power density and small size [1–4]. To achieve high-performance control in the above-mentioned fields, control methods for the PMSM include field-oriented control, sliding-mode control, model predictive control (MPC) [5–7], etc.

Compared with field-oriented control and sliding-mode control, MPC has the advantages of a simple structure and fast dynamic response [8, 9]. MPC mainly includes model predictive current control (MPCC), model predictive torque control, and deadbeat MPCC.

As an important branch of MPC, deadbeat MPCC has become a current research focus owing to its advantages such as fast dynamic response and small computational complexity [10]. Currently, it has been applied to PMSM control systems and has achieved good control in relevant research.

The performance of the MPC is highly dependent on the accuracy of the motor parameters. However, during motor operation, the parameters drift significantly due to factors such as temperature changes, permanent magnet magnetization, speed changes, and load disturbances, resulting in prediction errors and decrease in motor control performance.

Refs. [11–13] introduce an extended state observer (ESO) into MPC to reduce the impact of parameter mismatch on prediction accuracy. The experimental results show that this method can effectively improve the dynamic response performance and parameter robustness of a motor system. To reduce the impact of predictive model parameters on motor operation, ref. [14] proposes a novel model-free predictive current sliding-mode control strategy to achieve strong robustness of the system. Ref. [15] proposed the use of a sliding-mode disturbance observer to compensate for parameter disturbances and employed a feedforward controller with sliding-mode load compensation to replace the traditional PI controller. The experimental results verify that this method exhibits better dynamic response and current-tracking performance in the presence of disturbances. Considering the issue in MPC systems where computation delays in digital circuits lead to inaccurate current tracking, ref. [16] proposes a sensorless MPCC for PMSM based on delay compensation, which can effectively address this problem. To enhance the robustness of the MPC system, ref. [17] proposes a predictive control method based on an incremental PMSM model. This strategy designs a current disturbance observer based on the concept of incremental iteration to eliminate the influence of flux parameters on the motor. The experimental results demonstrate that this method can significantly reduce the steady-state current error caused by parameter mismatches. Ref. [18] proposes an improved delay compensation method. By predicting the current variation during the delay time and performing compensation, the calculation delay predicted by the model can be reduced. Compared with the traditional two-step delay compensation, this method makes it easier to achieve optimal control. In response to disturbances caused by parameter variations, refs. [19–22] propose using a Kalman filter to estimate changes in parameter disturbance while reducing the impact of motor noise. To address the issue of parameter mismatch affecting motor control performance in traditional deadbeat MPCC systems, refs. [23–25] propose a current error compensator. This method not only compensates for current errors in real time but also calculates the motor's inductance and flux linkage for effective parameter identification. The experimental results verify that this method ensures the ac-

* Corresponding author: Wan Chen (calvinchen@hau.edu.cn).

doi:10.2528/PIERC26061501

Published by THE ELECTROMAGNETIC ACADEMY

curacy of motor parameter identification and the robustness of the control system.

It is a significant challenge to improve the disturbance rejection performance of control systems. The main contribution of this paper is that a deadbeat MPCC scheme based on a disturbance observer is proposed, aiming to improve speed dynamic performance and enhance system robustness. To address the issue that conventional active disturbance rejection control (ADRC) employs only a single standard ESO, which exhibits low sensitivity to errors, an ESO incorporating a derivative term is introduced to enhance error sensitivity. However, the differential term will generate noise. This paper combines the advantages of both ESOs by taking a weighted average of the disturbance estimates from Observer 1 and Observer 2. Meanwhile, in the context of MPCC, parameter disturbance compensation is applied. Traditional ESO requires bandwidth parameter tuning, which is a complex process. This article proposes an ESO based on adaptive bandwidth, which can flexibly adjust the observer gain and enhance the accuracy of disturbance compensation.

2. MATHEMATICAL MODEL OF PMSM

Ignoring the motor's hysteresis and eddy current losses, the voltage equation of the surface-mounted PMSM is as follows:

$$\begin{cases} u_d = Ri_d + L\frac{di_d}{dt} - \omega_e L i_q \\ u_q = Ri_q + L\frac{di_q}{dt} + \omega_e L i_d + \omega_e \varphi_f \end{cases} \tag{1}$$

where u_d and u_q are voltage components; i_d and i_q are current components in the d-q coordinate system; ω_e is the electrical angular velocity; φ_f is the magnetic flux of the permanent magnet; R is the stator resistance; L is the winding inductance.

The electromagnetic torque and mechanical motion equations of the PMSM are as follows:

$$\begin{cases} T_e = \frac{3}{2} p_n \varphi_f i_q \\ J\frac{d\omega_m}{dt} = T_e - T_L - B\omega_m \end{cases} \tag{2}$$

where T_e is the electromagnetic torque; T_L is the load torque; p_n is number of pole pairs; J is the moment of inertia; B is the viscosity coefficient.

3. BASIC PRINCIPLE OF DEADBEAT MPCC

As the core unit of the motor drive system, the performance of the current controller directly determines the system's dynamic response and steady-state accuracy [26]. Compared with traditional field-oriented control, deadbeat MPCC has a faster response speed. Therefore, a deadbeat MPCC strategy based on a disturbance observer is proposed in this study. The structure of the traditional deadbeat MPCC system is shown in Fig. 1.

The deadbeat MPCC is based on a discrete mathematical model of the motor control system. First, the current value is sampled in real time during each control cycle, and the current value at current moment is used as a reference value. The optimal reference voltage vector is calculated using the discretized voltage equation, and switching signals for the inverter is then generated via space vector pulse width modulation. Ultimately,

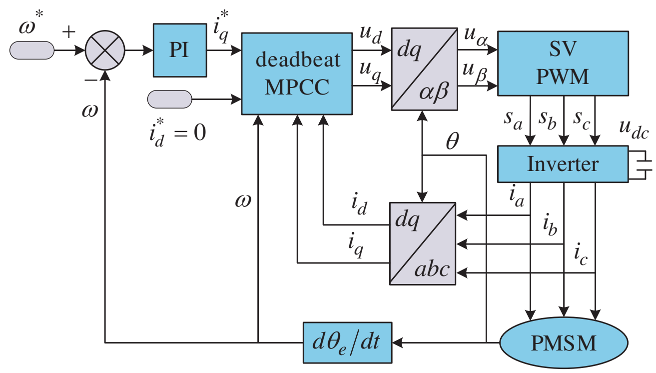

FIGURE 1. The traditional deadbeat MPCC system.

the system achieved zero static error tracking for the reference current. The discretized mathematical model is presented in Equation (3).

$$\begin{cases} u_d(k) = \frac{L}{T_s} i_d(k+1) + (R - \frac{L}{T_s}) i_d(k) \\ \qquad -\omega_e(k) L i_q(k) \\ u_q(k) = \frac{L}{T_s} i_q(k+1) + (R - \frac{L}{T_s}) i_q(k) \\ \qquad +\omega_e(k) L i_d(k) + \omega_e(k)\varphi_f \end{cases} \tag{3}$$

where $i_d(k)$ and $i_q(k)$ are the actual output currents; $i_d(k+1)$ and $i_q(k+1)$ are the given currents; T_s is the sampling time.

4. IMPROVED DEADBEAT MPCC SYSTEM

4.1. Simplified Active Disturbance Rejection Controller

To reduce overshoot of the speed and improve response speed, a simplified linear ADRC was designed to replace the traditional PI controller [27]. Its structure is illustrated in Fig. 2.

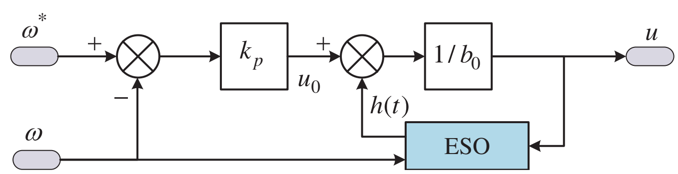

FIGURE 2. Block diagram of simplified linear ADRC.

Compared with traditional controllers, the ESO proposed in this study first uses two observers to estimate the disturbance values, respectively [28–30]. Then, the sum of the disturbances for the two observers can be calculated, and the average of the two observer values can be considered as the new disturbance. The new disturbance serves as an input to the observer, which can improve the accuracy of disturbance estimation. The observer gain is tuned using the bandwidth method [31].

The state equation shown in Equation (4) can be obtained from Equation (2).

$$\begin{cases} \dot{\omega}_m = \frac{3p_n\varphi_f}{2J} i_q - \frac{1}{J} T_L - \frac{B}{J}\omega_m + d(t) \\ \quad = b_0 u + f \\ f = -\frac{1}{J} T_L - \frac{B}{J}\omega_m + d(t) \end{cases} \tag{4}$$

where $b_0 = 1.5 p_n \varphi_f / J$ is the gain of the controller; $u = i_q$ is the output of the controller; $d(t)$ is an unknown disturbance; f is the disturbance except for $b_0 u$.

ω_m and f are expanded into new state variables x_{s1} and x_{s2}, respectively, as shown in Equation (5).

$$\begin{cases} x_{s1} = \omega_m \\ x_{s2} = f \\ \dot{x}_{s1} = x_{s2} + b_0 u \\ \dot{x}_{s2} = \dot{f} \end{cases} \tag{5}$$

Based on Equation (5), an improved extended state observer 1 can be established.

$$\begin{cases} e_{s1} = \omega_m - z_{s1} \\ \dot{z}_{s1} = z_{s2} + 2\omega_0 e_{s1} + b_0 u \\ \dot{z}_{s2} = \omega_0^2 e_{s1} + 2\omega_0 \dot{e}_{s1} \end{cases} \tag{6}$$

where z_{s1} is the speed estimation; z_{s2} is the disturbance estimation; ω_0 is the observer bandwidth.

Similarly, the mathematical model for observer 2 can be obtained as follows:

$$\begin{cases} e_1 = \omega_m - z_1 \\ \dot{z}_1 = b_0 u + 2\omega_0 e_1 + (z_2 + z_{s2})/2 \\ \quad\; = b_0 u + 2\omega_0 e_1 + h(t) \\ \dot{z}_2 = \omega_0^2 e_1 \end{cases} \tag{7}$$

where z_1 is the speed estimation; z_2 is the disturbance estimation; $h(t)$ is the average value of the total disturbance estimated by the two observers.

The improved ESO is shown in Fig. 3.

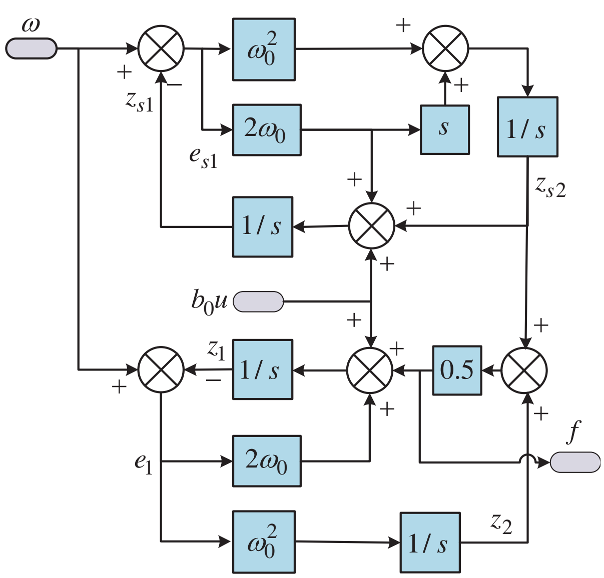

FIGURE 3. The ESO structure diagram.

The formula for proportional error feedback control rate is as follows:

$$\begin{cases} e = \omega_m^* - \omega_m \\ u_0 = k_p e \\ u = (u_0 - h(t)/b_0 \end{cases} \tag{8}$$

where ω_m^* is the expected mechanical angular velocity; e is the difference between the expected and actual speeds; u_0 is the control law; k_p is the proportional gain.

Based on Equation (6), the transfer function between z_{s2} and ω_m in observation 1 is obtained as:

$$G_{D1S}(s) = \frac{z_{s2}(s)}{\omega_m(s)} = \frac{2\omega_0 s^2 + \omega_0^2 s}{s^2 + 4\omega_0 s + \omega_0^2} \tag{9}$$

Based on traditional ESO, the disturbance of observer 1 is introduced as the input of observer 2. The transfer function between z_2 and ω_m in observer 2 is as follows:

$$G_{D2S}(s) = \frac{z_{s2}(s)}{\omega_m(s)} = \frac{\omega_0^2 s}{s^2 + 2\omega_0 s + \omega_0^2} \tag{10}$$

Observer 1 contains a second-order derivative term, indicating superior dynamic performance, whereas the conventional ESO exhibits relatively poor dynamic performance. Observer 2 synthesizes the advantages of both observers: it leverages the fast-tracking characteristic of observer 1 to compensate for the insufficiency of disturbance compensation in the conventional observer.

4.2. Analysis of MPCC Parameter Mismatch

The resistance, inductance, and magnetic flux change with variation in motor operating conditions, resulting in inaccurate prediction accuracy and subsequently affecting the performance of the control system. The MPCC's parameter mismatch is analyzed in the following section.

First, voltage Equation (1) is transformed into a current equation.

$$\begin{cases} \frac{di_d}{dt} = -\frac{R}{L} i_d + \frac{1}{L} u_d + \omega_e i_q \\ \frac{di_q}{dt} = -\frac{R}{L} i_q + \frac{1}{L} u_q - \omega_e i_d - \frac{1}{L}\omega_e \varphi_f \end{cases} \tag{11}$$

Discretize to obtain the current prediction equation, as follows:

$$\begin{cases} i_d(k+1) = (1 - \frac{RT_s}{L}) i_d(k) + \frac{T_s}{L} u_d(k) + T_s \omega_e i_q(k) \\ i_q(k+1) = (1 - \frac{RT_s}{L}) i_q(k) + \frac{T_s}{L} u_q(k) \\ \qquad -T_s \omega_e i_d(k) - T_s \omega_e \varphi_f \end{cases} \tag{12}$$

According to the current prediction equation in Equation (12), the deviation between the predicted model parameters and actual values is denoted as ΔR, ΔL, $\Delta\varphi_f$. The new current prediction equation is as follows:

$$\begin{cases} i_d'(k+1) = (1 - \frac{(R+\Delta R)T_s}{L+\Delta L}) i_d(k) \\ \qquad + \frac{T_s}{L+\Delta L} u_d(k) + T_s \omega_e i_q(k) \\ i_q'(k+1) = (1 - \frac{(R+\Delta R)T_s}{L+\Delta L}) i_q(k) + \frac{T_s}{L+\Delta L} u_q(k) \\ \qquad -T_s \omega_e i_d(k) - \frac{T_s(\varphi_f + \Delta\varphi_f)}{L+\Delta L} \omega_e \end{cases} \tag{13}$$

By subtracting Equation (12) from Equation (13), the current error of the MPCC can be obtained.

$$\begin{cases} \varepsilon_d = \frac{T_s R \Delta L - T_s L \Delta R}{L(L+\Delta L)} i_d(k) - \frac{T_s \Delta L}{L(L+\Delta L)} u_d(k) \\ \varepsilon_q = \frac{T_s R \Delta L - T_s L \Delta R}{L(L+\Delta L)} i_q(k) - \frac{T_s \Delta L}{L(L+\Delta L)} u_q(k) \\ \qquad + \frac{T_s \omega_e \varphi_f \Delta L - T_s \omega_e \Delta\varphi_f L}{L(L+\Delta L)} \end{cases} \tag{14}$$

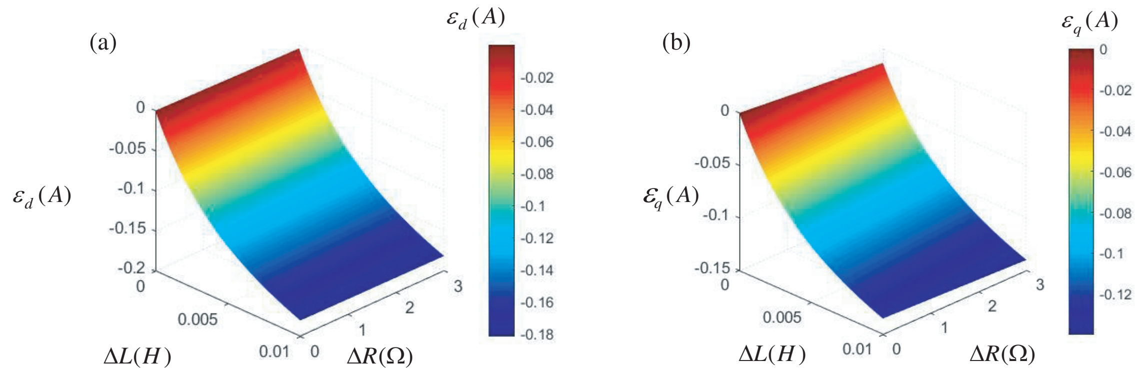

FIGURE 4. The influence of parameter error on current error: (a) the d-axis current error and (b) the q-axis current error.

where ε_d and ε_q are the current errors of the MPCC in the d-q coordinate system.

As shown in Fig. 4, the prediction error of the d-q coordinate current is mainly affected by the inductance error. If the resistance error is constant, the absolute value of the current error changes rapidly as the inductance error varies from 0 to 0.01, reaching a maximum of 0.18 A. If the inductance error is constant, the absolute value of the current error changes slowly, and the change is almost negligible.

5. PARAMETER DISTURBANCE COMPENSATION OBSERVER DESIGN

Through the analysis of parameter disturbances, the voltage equation with parameter disturbances can be obtained as follows:

$$\begin{cases} u_d = Ri_d + L\frac{di_d}{dt} - \omega_e L i_q + G_d \\ u_q = Ri_q + L\frac{di_q}{dt} + \omega_e L i_d + \omega_e \varphi_f + G_q \\ G_d = \Delta L\frac{di_d}{dt} + \Delta R i_d - \Delta L \omega_e i_q \\ G_q = \Delta L\frac{di_q}{dt} + \Delta R i_q + \Delta L \omega_e i_d + \Delta\varphi_f \omega_e \end{cases} \tag{15}$$

where G_d and G_q are disturbances caused by the parameters.

The voltage equation is transformed into the current equation as follows:

$$\begin{cases} \frac{di_d}{dt} = -\frac{R}{L} i_d + \frac{1}{L} u_d + \omega_e i_q - \frac{1}{L} G_d \\ \frac{di_q}{dt} = -\frac{R}{L} i_q + \frac{1}{L} u_q - \omega_e i_d - \frac{1}{L}\omega_e \varphi_f - \frac{1}{L} G_q \end{cases} \tag{16}$$

Let $g_d = -\frac{1}{L} G_d$, $g_q = -\frac{1}{L} G_q$, the parameter perturbation equation is as follows:

$$\begin{cases} g_d = -\frac{1}{L}(\Delta L\frac{di_d}{dt} + \Delta R i_d - \Delta L \omega_e i_q) \\ g_q = -\frac{1}{L}(\Delta L\frac{di_q}{dt} + \Delta R i_q + \Delta L \omega_e i_d + \Delta\varphi_f \omega_e) \end{cases} \tag{17}$$

where g_d is the d-axis component of the disturbance at current equation, and g_q is the q-axis component of the disturbance at current equation.

The mathematical model for the deadbeat MPCC considering the influence of parameter changes can be written as:

$$\begin{cases} u_d(k) = \frac{L}{T_s} i_d(k+1) + (R - \frac{L}{T_s}) i_d(k) \\ \quad -\omega_e(k) L i_q(k) - L g_d \\ u_q(k) = \frac{L}{T_s} i_q(k+1) + (R - \frac{L}{T_s}) i_q(k) \\ \quad +\omega_e(k) L i_d(k) + \omega_e(k)\varphi_f - L g_q \end{cases} \tag{18}$$

To improve parameter robustness and reduce current ripple, an extended state observer was designed to estimate the total disturbance and compensate for the deadbeat MPCC.

$$\text{Let } I_{11} = [i_d, i_q]^T, \quad g(t) = [g_d(t), g_q(t)]^T,$$
$$u = [u_d + \omega_e L i_q, u_q - \omega_e L i_d - \omega_e \varphi_f]^T$$

$$A = \begin{bmatrix} -\frac{R}{L} & 0 \\ 0 & -\frac{R}{L} \end{bmatrix}, \quad B = \begin{bmatrix} \frac{1}{L} & 0 \\ 0 & \frac{1}{L} \end{bmatrix}$$

By combining Equations (16) and (17), the current state equation can be obtained as follows:

$$\begin{cases} \dot{I}_{11} = A I_{11} + Bu + g(t) \\ \dot{g}(t) = r(t) \end{cases} \tag{19}$$

Based on Equation (19), the current expansion state observer is designed as follows:

$$\begin{cases} \dot{z}_{11} = A z_{11} + Bu + z_{21} - \beta_1 e_1 \\ \dot{z}_{21} = -\beta_2 e_1 \\ e_1 = z_{11} - I_{11} \end{cases} \tag{20}$$

where $z_{11} = \begin{bmatrix} z_{1d} & z_{1q} \end{bmatrix}^T$ is the current estimation; $z_{21} = \begin{bmatrix} z_{2d} & z_{2q} \end{bmatrix}^T$ is the disturbance estimation; β_1 and β_2 are the observer gains; e_1 is the error between the estimated and actual currents.

From Equations (19) and (20), the error state equation is obtained as follows:

$$\begin{cases} \dot{e}_1 = A e_1 + e_2 - \beta_1 e_1 \\ \dot{e}_2 = -\beta_2 e_1 - r(t) \\ e_1 = z_{11} - I_{11} \\ e_2 = z_{21} - g(t) \end{cases} \tag{21}$$

where e_2 is the error between the estimated and actual disturbances

Assuming that the upper limit of the disturbance change rate remains within a certain range for a short period of time, namely $|\dot{g}(t)| \le G$, the transfer function can be obtained based on the current error and disturbance as follows:

$$\frac{E(s)}{G(s)} = -\frac{s}{s^2 + (\beta_1 - A)s + \beta_2} \tag{22}$$

Let $\beta_1 - A = 2\omega_{c0}$, $\beta_2 = \omega_{c0}^2$, and the following expression can be obtained.

$$\frac{E(s)}{G(s)} = -\frac{s}{s^2 + 2\omega_{c0}s + \omega_{c0}^2} \tag{23}$$

where ω_{c0} denotes the bandwidth gain of the current observer.

Since $\dot{g}(t) = r(t)$, the expression can be written as

$$\frac{E(s)}{R(s)} = -\frac{1}{s^2 + 2\omega_{c0}s + \omega_{c0}^2} \tag{24}$$

Equation (22) can be converted into the frequency domain expression

$$\left|\frac{E(s)}{R(s)}\right|_{s=j\omega} = \frac{1}{\omega^2 + \omega_{c0}^2} \tag{25}$$

Using the scaling method, the following relationship can be obtained:

$$|E(s)|_{s=j\omega} \le \frac{1}{\omega_{c0}^2}\,|R(j\omega)| \tag{26}$$

From $|\dot{g}(t)| \le G$, $|e_{1m}| \le \frac{G}{\omega_{c0}^2}$ can be obtained.

If the disturbance changes, I_{11} will also change. I_{11} is obtained via coordinate transformation and is also related to the back electromotive force.

$$\dot{E} = \begin{bmatrix} \dot{e}_\alpha \\ \dot{e}_\beta \end{bmatrix} = \begin{bmatrix} -\omega_e^2\varphi_f \cos\theta_e \\ \omega_e^2\varphi_f \sin\theta_e \end{bmatrix} \tag{27}$$

Maximum current error is

$$|e_1|_{\max} \le \left|\dot{E}\right|_{\max} = \frac{\omega_e^2\varphi_f}{\omega_{c0}^2} \tag{28}$$

Based on Equation (28), the adaptive bandwidth can be obtained as:

$$\omega_{c0} = \omega_e\sqrt{\frac{\varphi_f}{|e_1|_{\max}}} \tag{29}$$

where $|e_1|_{\max}$ is a constant value representing the maximum current error between the estimated and actual currents.

As long as the gain k is a finite constant (i.e., $|k| < \infty$), for any bounded input $|x(t)| \le M < \infty$, the output is necessarily bounded: $|y(t)| = |k| \cdot |x(t)| \le |k| \cdot M < \infty$. The system is bounded-input bounded-output (BIBO) stable if and only if k is finite. If $k = \infty$, it is unstable (which does not exist in practice).

The mathematical model of the d-axis adaptive disturbance observer is as follows:

$$\begin{cases} \dot{z}_{1d} = Az_{1d} + Bu + z_2 - 2\omega_{c0}e_{1d} \\ \dot{z}_{2d} = -\omega_{c0}^2 e_{1d} \\ e_{1d} = z_{1d} - i_d \end{cases} \tag{30}$$

The structural diagram of the d-axis continuous adaptive disturbance observer is shown in Fig. 5.

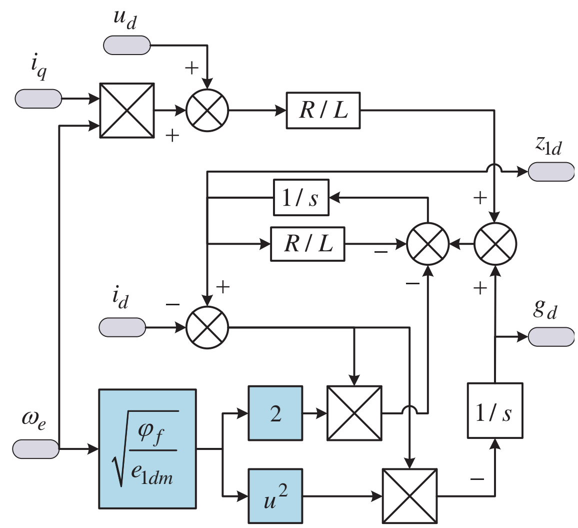

FIGURE 5. The d-axis adaptive disturbance observer.

Similarly, the q-axis disturbance observer can be obtained as follows.

The mathematical model of the d-axis adaptive disturbance observer is discretized as follows:

$$\begin{cases} e_{1d} = z_{1d}(k) - i_d(k) \\ z_{1d}(k+1) = (1 - \frac{R}{L}T_s)z_{1d}(k) + \frac{T_s}{L}u_d(k) \\ \qquad +T_s\omega_e(k)i_q(k) + T_s z_{2d}(k) \\ \qquad -2\omega_{c0}T_s e_{1d} \\ z_{2d}(k) = z_{2d}(k) - \omega_{c0}^2 T_s e_{1d} \end{cases} \tag{31}$$

where $e_{1d}(k)$ is the error between the estimated and actual currents; T_s is the sampling time; $z_{1d}(k)$ is the estimated current; $i_d(k)$ is the actual current.

A diagram of the deadbeat MPCC system based on a disturbance observer is shown in Fig. 6.

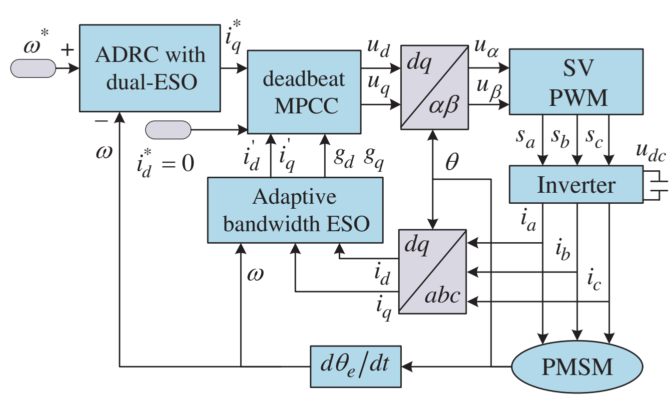

FIGURE 6. The improved deadbeat MPCC system for PMSM.

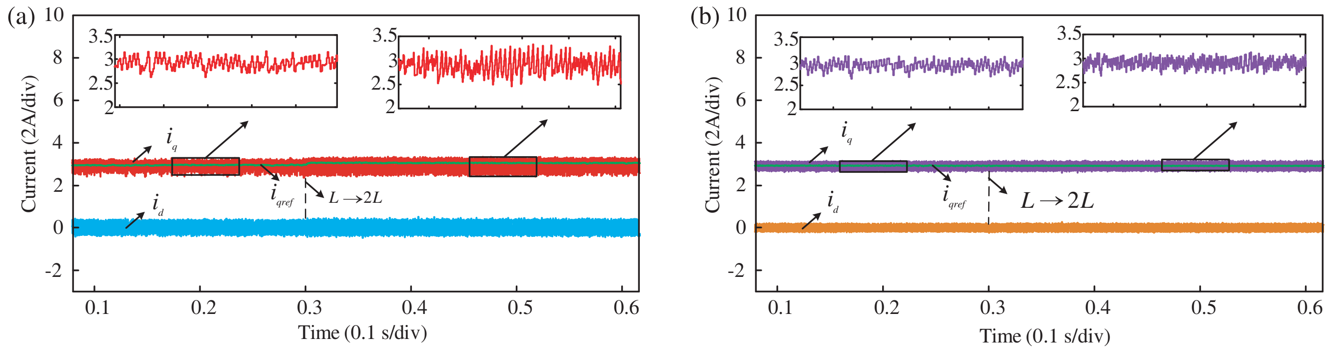

FIGURE 7. Simulation comparison of current waveforms: (a) traditional deadbeat MPCC and (b) improved deadbeat MPCC.

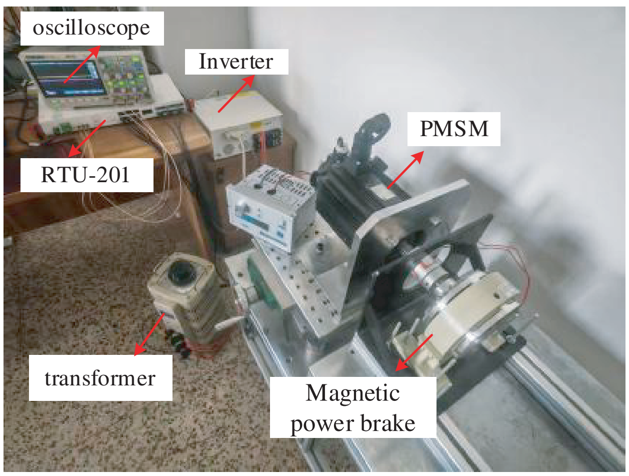

FIGURE 8. Experimental platform.

6. SIMULATION AND EXPERIMENTAL VERIFICATION

The motor control performance of the proposed control strategy was verified. The simulation and experimental results are presented for comparative analysis. In the traditional strategy, k_p is 0.14, and k_i is 6.4. For the improved self-disturbance control, k_p is 300, and the ESO bandwidth is 300. For the current disturbance observer, the bandwidth is 1500. The actual load torque is $5\,\mathrm{N \cdot m}$.

6.1. Simulation Analysis

The simulation results for the mismatch of inductance under a speed of 1000 r/min and rated load $5\,\mathrm{N \cdot m}$ are presented in Fig. 7.

Figure 7 shows a comparison of current waveforms for the two control strategies as the stator inductance changes from L to $2L$. From the waveforms, it can be seen that the current fluctuation of the deadbeat MPCC is significant, and the q-axis current fluctuates from 24 A to 3.4 A. The q-axis current fluctuation range of the improved control strategy was maintained at a small range, fluctuating from 2.6 to 3.1 A.

Through simulation comparison, similar results can be obtained regarding the mismatch of parameters such as resistance and magnetic flux.

TABLE 1. Motor parameters.

Parameter	Value
Resistance	$2.857\,\Omega$
Inductance	8.5 mH
Viscous Friction Coefficient	$0.008\,\mathrm{N \cdot m \cdot s}$
Pole-pairs	4
Rotor Flux Linkage	0.175 Wb
Inertia of the Rotor	$0.003\,\mathrm{kg \cdot m^2}$
Rated voltage	380 V
Rated Torque	$15\,\mathrm{N \cdot m}$

6.2. Experimental Verification

To further validate the effectiveness of the proposed method, a comparative analysis of the experimental waveforms is presented, including speed-tracking and load disturbance rejection performance. The experimental platform is shown in Fig. 8. The experimental platform included a controller, inverter, transformer, PMSM, and magnetic powder brake. The motor parameters are shown in Table 1. The sampling frequency is 10 kHz.

Figure 10 shows speed waveforms for the two control strategies. The speed was varied from 200 r/min to 400 r/min. From the figure, it can be seen that the speed overshoot of the deadbeat MPCC control strategy is 20 r/min, and the response recovery time is 0.5 s, while the overshoot of the improved control strategy is very small, and the response recovery time is 0.18 s.

Figure 10 shows speed waveforms under the two control strategies for loading and unloading $5\,\mathrm{N \cdot m}$ at 300 r/min. From Fig. 10, it can be seen that the speed of the deadbeat MPCC decreases by approximately 35 r/min at the moment of loading, and when unloading, the speed increases by approximately 23 r/min. By adopting an improved control strategy, the speed decreased by approximately 15 r/min during loading and increased by approximately 12 r/min during unloading.

From Figs. 9 and 10, it can be seen that the improved control strategy can achieve no overshoot in speed and has a faster response speed. Compared with traditional PI controllers, the improved controller has stronger disturbance-rejection performance.

Figure 11 shows current waveforms of the two different control strategies during loading and unloading at a speed

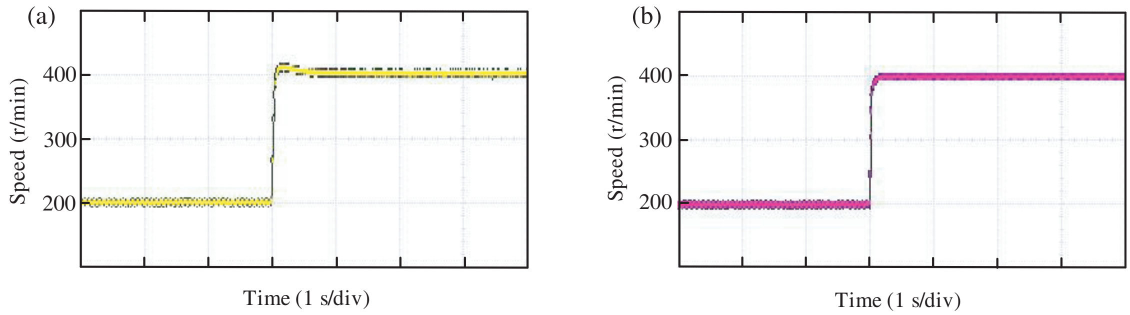

FIGURE 9. Speed tracking comparison: (a) traditional deadbeat MPCC and (b) improved deadbeat MPCC.

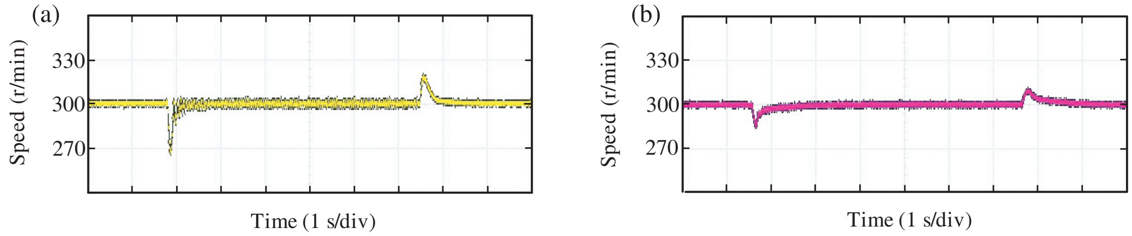

FIGURE 10. Speed waveforms under load disturbance: (a) traditional deadbeat MPCC and (b) improved deadbeat MPCC.

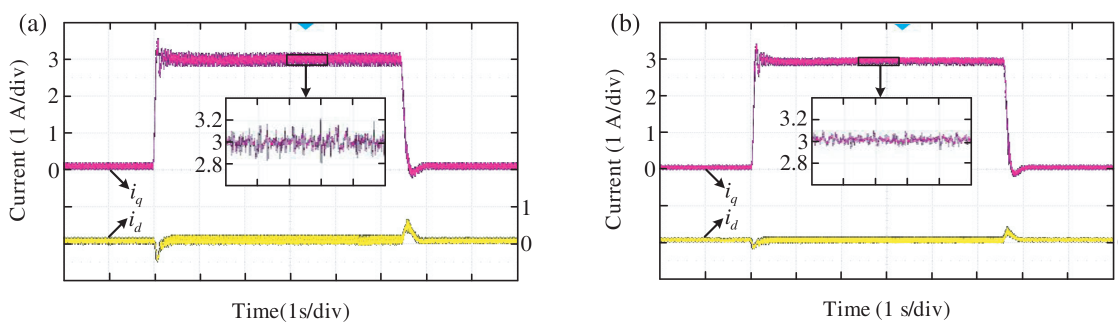

FIGURE 11. Current waveforms comparison under load variation conditions: (a) traditional deadbeat MPCC and (b) improved deadbeat MPCC.

of 200 r/min. According to Fig. 11, at the moment of load change, the maximum d-axis current fluctuation using the deadbeat MPCC method is approximately 0.8 A, and the maximum current fluctuation of the improved control strategy is approximately 0.5 A. The q-axis current exhibits a similar phenomenon. The current fluctuation of the improved control strategy was significantly smaller than the traditional method. From the waveforms in Fig. 11, it can be seen that compared with the deadbeat MPCC, the current fluctuation under the improved control strategy is significantly smaller than under load disturbances, indicating better load disturbance rejection performance.

7. CONCLUSION

This study proposes an improved deadbeat MPCC strategy for PMSM based on a disturbance observer to enhance disturbance-rejection capability and MPCC's parameter robustness. An active disturbance rejection controller was designed to replace the PI control. A disturbance observer with an adaptively adjustable gain is designed. Parameter mismatch disturbances can be compensated. The experimental results show that a simplified linear ADRC speed regulator can achieve both a fast response and overshoot suppression during speed changes. The disturbance observer can significantly suppress current ripple and exhibits better robustness in the presence of external disturbances and parameter mismatches.

ACKNOWLEDGEMENT

This work was funded by the Sci&Tech Program of Huai'an under Grant No. HAG202302.

REFERENCES

[1] Kou, B., X. Zhao, H. Zhang, and M. Wang, "Review and analysis of electromagnetic structure and magnetic field regulation technology of the permanent magnet synchronous motor," *Proceedings of the CSEE*, Vol. 41, No. 20, 7126–7141, 2021.

[2] Ke, D., F. Wang, and J. Li, "Predictive current control of permanent magnet synchronous motor based on an adaptive high-gain observer," *Proceedings of the CSEE*, Vol. 41, No. 2, 728–738, 2021.

[3] Lu, Q. and F. Wu, "Sensorless control strategy for permanent magnet synchronous motor based on intermediate function dis-

turbance observer," *Journal of Power Electronics*, Vol. 26, 620–628, 2026.

[4] Wang, Y., C. Zhang, and W. Hao, "Overview of fault-tolerant technologies of permanent magnet brushless machine and its control system," *Proceedings of the CSEE*, Vol. 42, No. 1, 351–372, 2022.

[5] Diab, A. A. Z. and D. A. Kotin, "Speed and current vector controlled permanent magnet synchronous motor drive based on particle SWARM optimization," in *2022 IEEE 23rd International Conference of Young Professionals in Electron Devices and Materials (EDM)*, 576–583, Altai, Russian Federation, 2022.

[6] Chen, W., S. Zeng, G. Zhang, T. Shi, and C. Xia, "A modified double vectors model predictive torque control of permanent magnet synchronous motor," *IEEE Transactions on Power Electronics*, Vol. 34, No. 11, 11 419–11 428, Nov. 2019.

[7] Ding, H., X. Zou, and J. Li, "Sensorless control strategy of permanent magnet synchronous motor based on fuzzy sliding mode observer," *IEEE Access*, Vol. 10, 36 743–36 752, 2022.

[8] Xu, Q., X. Long, Y. Miao, Y. Wang, Y. Tu, and M. Tang, "Double-vector model predictive current control for PMSM drive system with low calculation burden," *Electric Machines and Control*, Vol. 29, No. 5, 19–30, 2025.

[9] Guo, Y., F. Jiang, S. Wang, S. Cheng, and Z. Hu, "Variable control period model predictive current control with current hysteresis for permanent magnet synchronous motor drives," *Actuators*, Vol. 14, No. 11, 517, 2025.

[10] Zhang, X., Z. Wang, and H. Bai, "Sliding-mode-based deadbeat predictive current control for PMSM drives," *IEEE Journal of Emerging and Selected Topics in Power Electronics*, Vol. 11, No. 1, 962–969, 2023.

[11] Dai, J., L. Liu, J. Ahn, J. Lee, and H. Kim, "Extended state observer-based deadbeat predictive current control for IPMSM enhancing full parameter robustness," *IEEE Transactions on Industry Applications*, Vol. 61, No. 6, 9347–9358, 2025.

[12] Zhang, G., X. Yao, X. Gao, and Z. Li, "Model-free deadbeat direct speed control with adaptive bandwidth factor in surface-mounted permanent magnet synchronous motor," *IEEE Journal of Emerging and Selected Topics in Power Electronics*, Vol. 14, No. 2, 2527–2540, 2026.

[13] Li, M., J. Zhao, Y. Hu, and Z. Wang, "Active disturbance rejection position servo control of PMSLM based on reduced-order extended state observer," *Chinese Journal of Electrical Engineering*, Vol. 6, No. 2, 30–41, 2020.

[14] Wei, Y., H. Xie, D. Ke, and F. Wang, "Model-free predictive current sliding mode control strategy on PMSM drives based on universal model with PIDD2 causality," *Proceedings of the CSEE*, Vol. 45, No. 14, 5669–5679, 2025.

[15] Xu, Y., Z. Yan, Y. Zhang, and R. Song, "Model predictive current control of permanent magnet synchronous motor based on sliding mode observer with enhanced current and speed tracking ability under disturbance," *IEEE Transactions on Energy Conversion*, Vol. 38, No. 2, 948–958, 2023.

[16] Gong, C., L. Ding, Y. Li, and J. Li, "Improved sensorless FCS-MPCC with current pre-estimation-based delay compensation integrated for PMSMs over high-speed range," *IEEE Transactions on Industry Applications*, Vol. 59, No. 6, 6756–6765, 2023.

[17] Wang, S., Y. Hu, J. Zhao, and Y. Zhang, "Parameter robustness improvement of predictive current control for permanent-magnet synchronous motors," *IEEE Journal of Emerging and Selected Topics in Power Electronics*, Vol. 10, No. 2, 1619–1626, 2022.

[18] Gao, J., C. Gong, W. Li, and J. Liu, "Novel compensation strategy for calculation delay of finite control set model predictive current control in PMSM," *IEEE Transactions on Industrial Electronics*, Vol. 67, No. 7, 5816–5819, 2020.

[19] Yang, R., M. Wang, L. Li, G. Wang, and C. Zhong, "Robust predictive current control of PMLSM with extended state modeling based Kalman filter: For time-varying disturbance rejection," *IEEE Transactions on Power Electronics*, Vol. 35, No. 2, 2208–2221, 2020.

[20] Naas, B., L. Nezli, M. Elbar, and I. Zaitsev, "Speed estimation of a double-star permanent magnet synchronous motor using an optimized extended Kalman filter," *International Transactions on Electrical Energy Systems*, Vol. 2025, No. 1, 8466428, 2025.

[21] Kong, X. and Q. Yuan, "Disturbance-rejection control of permanent magnet synchronous motors using robust adaptive extended Kalman filter," *IEICE Electronics Express*, Vol. 22, No. 18, 20250397, 2025.

[22] Zhou, Y., S. Zhang, C. Zhang, X. Li, X. Li, and X. Yuan, "Current prediction error based parameter identification method for SPMSM with deadbeat predictive current control," *IEEE Transactions on Energy Conversion*, Vol. 36, No. 3, 1700–1710, 2021.

[23] Sun, X., S. Zhang, Z. Yang, G. Lei, and T. Li, "Improved DPCC and parameter identification for permanent magnet synchronous motors with current error compensation," *IEEE Transactions on Industrial Electronics*, Vol. 72, No. 10, 9911–9921, 2025.

[24] Xie, C., S. Zhang, X. Li, Y. Zhou, and Y. Dong, "Parameter identification for SPMSM with deadbeat predictive current control using online PSO," *IEEE Transactions on Transportation Electrification*, Vol. 10, No. 2, 4055–4064, 2024.

[25] Zhong, S., L. Zheng, and G. Xiang, "Parameter identification method for permanent magnet synchronous motors based on model reference adaptive system," *Journal of Innovation and Development*, Vol. 12, No. 1, 59–64, 2025.

[26] Xu, A., Y. Yu, and R. Liu, "Deadbeat control of permanent magnet-assisted synchronous reluctance motor based on LESO," *Electric Machines and Control*, Vol. 29, No. 8, 116–128, 2025.

[27] Tian, M., B. Wang, Y. Yu, and D. Xu, "Speed fluctuations suppression strategy for PMSM based on resonance-improved single-degree-of-freedom active disturbance rejection controller," *Proceedings of the CSEE*, Vol. 44, No. 15, 6209–6219, 2024.

[28] Li, L., G. Pei, J. Liu, P. Du, L. Pei, and C. Zhong, "2-DOF robust H_∞ control for permanent magnet synchronous motor with disturbance observer," *IEEE Transactions on Power Electronics*, Vol. 36, No. 3, 3462–3472, 2021.

[29] Zhan, B., L. Zhang, Y. Liu, and J. Gao, "Model predictive and compensated ADRC for permanent magnet synchronous linear motors," *ISA Transactions*, Vol. 136, 605–621, 2023.

[30] Yuan, F. and H. Xiong, "Research on vector control of permanent magnet synchronous motor based on active disturbance rejection," in *2023 9th International Conference on Electrical Engineering, Control and Robotics (EECR)*, 202–206, Wuhan, China, 2023.

[31] Wang, B., M. Tian, Y. Yu, Q. Dong, and D. Xu, "Enhanced ADRC with quasi-resonant control for PMSM speed regulation considering aperiodic and periodic disturbances," *IEEE Transactions on Transportation Electrification*, Vol. 8, No. 3, 3568–3577, 2022.